ASIAN J NAT PROD BIOCHEM
Volume 21, Number 2, December 2023
Pages: 88-100

E-ISSN: 2580-2550
DOI: 10.13057/biofar/f210205

Anticancer activity of secondary metabolite isolated from the rhizospheric fungus *Fusarium oxysporum* isolate-*ABRF1*, 2-propenoic acid, pentadecyl ester

MAHENDRA KUMAR SAHU[1], SHRUTHI SUTHAKARAN[2,3], SHARMISTHA CHAITALI GHOSH[1], DIGVIJAY SINGH[2,3], AMITAVA DAS[2,3], HARIT JHA[1,♥]

[1]Department of Biotechnology, Guru Ghasidas Vishwavidyalaya. Bilaspur 495009, Chhattisgarh, India. Tel.: +91-7752-260356, ♥email: harit.jha@ggu.ac.in

[2]Department of Applied Biology, CSIR-Indian Institute of Chemical Technology. Uppal Road, Tarnaka, Hyderabad 500007, TS, India. Tel.: +91-402719-3143, ♥♥email: amitavadas.iict@gov.in

[3]Academy of Scientific and Innovative Research (AcSIR). Ghaziabad, UP 201002, India

Manuscript received: 30 June 2023. Revision accepted: 31 December 2023.

Abstract. *Sahu MK, Suthakaran S, Ghosh SC, Singh D, Das A, Jha H. 2023. Anticancer activity of secondary metabolite isolated from the rhizospheric fungus* Fusarium oxysporum *isolate-ABRF1, 2-propenoic acid, pentadecyl ester. Asian J Nat Prod Biochem 21: 88-100.* The rhizospheric fungus *Fusarium oxysporum ABRF1* from the Achanakmar Biosphere Reserve, Chhattisgarh, India, was evaluated for its anticancer potency using various cellular and molecular assays. A differential cytotoxic profile of the different fractions of the *ABRF1* isolate was observed against various cancer cell lines. DNA fragmentation analysis revealed the aqueous and toluene fractions were effective and correlated well with apoptotic gene expression in several breast cancer cells. The fractions showed markedly increased expression of pro-apoptotic protein markers – BAX and cleaved caspase 3 in the breast cancer cells. Structural and functional characterization of potential secondary metabolite from the fungal isolate *ABRF1* was carried out using Gas Chromatography with Mass Spectroscopy and Nuclear Magnetic Resonance that characterized as 2-propenoic acid, pentadecyl ester. The underlying mechanisms responsible for the anticancer property were confirmed by molecular docking analysis of 2-propenoic acid, pentadecyl ester, and positive controls such as Doxorubicin and Noscapine. The results showed an efficient binding with molecular targets such as protein kinases (EphA2) and epithelial-to-mesenchymal transition markers (Vimentin) in breast cancer cells. The active metabolite 2-propenoic acid, pentadecyl ester, has a potential anticancer property that needs to be taken further for in vivo studies and drug development in the future.

Keywords: Anticancer activity, *Fusarium*, molecular docking, rhizospheric range, secondary metabolite

INTRODUCTION

The quest and search for therapeutic agents have encouraged researchers on their expedition to the most unexplored spots of nature. Fungi are the most preferred source because of the production of secondary metabolites, which have the potential as medicines for various diseases (Demain and Fang 2000). Secondary metabolites provide greater structural diversity and opportunities to discover new molecules (Arnott and Planey 2012). The proportion of natural products or their derivatives is approximately 30% of currently available drugs (Gkarmiri et al. 2017). The ease of extraction of significant fungal metabolites has paved the way for their utilization and rigorous exploration along with herbal plants. The screening, identification, and isolation of bioactive compounds are essential to meet the increasing demand for natural medicines. The microbiome in the rhizospheric region plays diverse functions in plant nutritional uptake and recycling (Berg and Koskella 2018), coping with biotic and abiotic stresses (Bakker et al. 2018; Compant et al. 2019), activation of plant defense system during the onset of infection (Castillo-González and Zhang, 2018), nitrogen mineralization (Leach et al. 2017), attracting insect pollinators (Kaiser 2006), etc. The microbiota develops competitive strategies and cooperative behaviors at intra- and inter-species levels for fulfilling nutritional requirements. They withstand ecological turbulence when cohabitating in the phyllosphere, endorhizosphere, and ectorhizosphere of soil (Hibbing et al. 2000).

Rhizospheric fungi are microorganisms that spend the whole or part of their lifecycle residing symbiotically within the healthy root tissues of higher host plants and mimic the chemistry of their respective hosts. Fungi produce various extracellular enzymes such as cellulases, amylases, pectinases, laccases, lipases, and proteinases (Meligy et al. 2014; Sahu et al. 2023a,b). These fungal enzymes play a crucial role in biodegradation and hydrolysis processes and are important against pathogenic infection and in fulfilling the nutritional needs of the host plants (Pinton et al. 2010). The rhizosphere range of the fungus produces many secondary metabolites with a biological activity that may be harmful to other organisms, such as mycotoxins and phytotoxins, or beneficial, such as antibiotics and other pharmaceuticals. These compounds interact with microorganisms, plant cells, and other fungi (Miranda et al. 2010). Secondary metabolites can regulate the prokaryotic cells and the metabolism of other fungus and plant cells. Synthesis of these low molecular weight

compounds is not required for normal growth of the fungus; however, these compounds may provide several benefits to the organism (Sahu and Jha 2020a,b). Volatile organic compounds synthesized by fungi possess antimicrobial properties and thus regulate the diversity and population of the microbiome (Dreher et al. 2019). Metabolic exchange in regulating microbial interaction involves complex regulatory mechanisms that drive the secondary metabolite biosynthesis. Bioactive secondary metabolites produced by the rhizospheric fungal communities are fundamental to various processes, such as *Trichoderma harzianum* used as a biocontrol agent, aids transport metals, antifungal, stimulates plant growth, and enhances plant biomass (Vinale et al. 2012; Braga et al. 2016). They also boost systemic disease resistance against phytopathogens, suppress necrosis in leaves, alter the plant hormone metabolism, etc. (Sarsaiya et al. 2019). Progress in the characterization of these secondary metabolites for the benefit of humanity has been progressing very slowly. The use of fungal-derived bioactive compounds as vital natural pharmaceutical biomolecules, specifically targeting anticancer properties, has been established in this study. Despite their importance and benefits, research on these fungal metabolites is limited.

Recent studies showed several bioactive compounds, including antifungal and antibacterial agents, have been isolated from fungi (Sahu et al. 2020). The promotion of plant growth is the significant contribution of fungal symbiosis. This study examined a Fusarium species isolated from untapped soil of the Achanakmar forest of Chhattisgarh (India) for its various biological properties. The crude extract of pure isolates was chosen for purification of their secondary metabolites using chromatography techniques (TLC, HPLC, GC–MS) that were then subjected to nuclear magnetic resonance (NMR) to test them for their in-vitro anticancer properties along with in-silico molecular docking was performed to strengthen the study.

MATERIALS AND METHODS

Chemicals and reagents

The solvents were of analytical grade and purchased from Merck, Germany. Potato Dextrose Agar (PDA), Czapek Dox Agar, and Potato Dextrose Broth were obtained from HiMedia, India. Doxorubicin, 2,2'azinobis (3-ethyl benzothiazole-6-sulphonic acid), and other molecular biology reagents were procured from Sigma-Aldrich, USA. Deionized water (Millipore, USA) was used throughout the experiment.

Fungal isolation and identification

Rhizospheric fungi were collected from the rhizospheric region of soil from the Achanakmar Biosphere (Bilaspur) in the central mainland of the Indian subcontinent renowned as "Herbal State-Chhattisgarh" by the method of (Radhika and Rodrigues 2010). The fungus was identified and characterized as described previously by (Sahu et al. 2020).

Extraction

Fusarium oxysporum (Isolate *ABRF1*) was initially incubated at 25 ±2°C for 15-20 days to obtain the maximum biomass of the fungus. After incubation, to obtain the promising secondary metabolites, the cultured biomass was treated with 1.5% Triton X-100 (v/v) and incubated under shaking conditions at 100 rpm for 30 min. It helped disrupt the cell wall to enhance the release of intracellular secondary metabolites. (Lin et al. 1976; McGhee et al. 1982; Robinson et al. 2001; Soccol et al. 2017). The culture media was filtered to separate the secondary metabolites from the fungal biomass (Alkhulaifi et al. 2019; Sharma et al. 2016). The collected filtrate was concentrated up to 20% of the original volume (v/v) using a vacuum rotary evaporator at 50±5°C. The concentrated extract was stored at 4°C. The working solution was prepared for subsequent experiments by diluting the concentrated extract in sterilized distilled water.

Solvent extraction process

Fungal biomass was subjected to solvent extraction using ethanol to obtain secondary metabolites. Dried ethanolic extract was purified using column chromatography with a silica gel mesh size of 60-120. One g of fungal crude extract was dissolved in ethanol (1:1 w/v) and was loaded on the column. Increasingly, polar solvents were used for elution. Every fraction was collected and spectrophotometrically evaluated. Crude ethanolic extract was purified using various eluents ranging from polar to non-polar solvents, i.e., acetonitrile, ethyl acetate, methanol, chloroform, and toluene. The fraction with maximum activity was purified further to obtain a pure compound. The ethanol used in the Soxhlet extractor was of analytical grade, and the fraction obtained was concentrated and dried in a sterilized condition.

Biochemical assay

The dried extract was dissolved in 1% DMSO (Dimethyl sulphoxide) in PBS (Phosphate buffer saline) and vortex for 1 min. Phytochemical analysis was conducted using the supernatant obtained after centrifugation at 100 g for 2 min., as described by Sahu et al. (2023a,b).

Purification of the ethanolic extract

Thin-Layer Chromatography (TLC)

TLC was used to separate the compounds of *F. oxysporum* ethanolic extract. Different column fractions of the ethanolic extract were loaded on thin-layer silica gel plates, and separation was carried out in an ascending TLC manner (Azerang et al. 2019). The ethanolic crude extract and its relatively pure column fractions from isolate *ABRF1* were spotted on a silica TLC and visualized using UV - 366 nm. The varying concentration of the mobile phase of the solvent system, i.e., Acetonitrile: Water: Acetic acid at a ratio of 18:80:2 v/v, accelerated the release of different compounds from the extract. The air-dried chromatogram was subjected to an iodine chamber to evaluate the TLC profile. Fractions with similar TLC profiles were pooled together, and forming a single spot suggested the relative purity of the compound.

High-Performance Liquid Chromatography (HPLC) analysis

The purity of the secondary metabolites was validated by HPLC using a C_{18} column (Shimadzu Liquid Chromatography LC10A; Shimadzu Corp. Kyoto, Japan). HPLC-grade methanol was used as a solvent for dissolving the extract in a ratio of 1:1 w/v. 20µl sample was injected, and the elution flow rate was set at 1mL/min through mobile (an isocratic) phase, i.e., Acetonitrile: Water: Acetic acid at the ratio 18:80:2 v/v. The chromatogram profile was analyzed at 280 nm. A calibration curve was prepared using standard catechin and phloroglucinol (200 ppm/10 µl of injection volume) as described in (Shen et al. 2007).

Spectroscopic method of compound identification

Fourier Transform Infrared (FTIR) spectroscopy

FTIR spectroscopy was carried out (Bhat 2013; D'Souza and Kamat 2017) to determine functional groups present in the extract. FTIR spectrometer was used to record the infrared transmittance at a wavenumber ranging from 4000-400 cm^{-1} of the purified compounds (FTIR, I05 Nicolet Avatar 370, Thermo Scientific, USA). Next, 5 mg of the pure compound was mixed with 95 mg KBr spectroscopic grade for pellet preparation. The pellet and control KBr pellets were used for analysis.

Gas Chromatography-Mass Spectroscopy (GC-MS)

The qualitative and quantitative analysis of the compounds in the extract was carried out using Shimadzu GC-MS-QP2020, Kyoto, Japan. The electron impact ionization was taken at 70eV, and the mass ranged from 40-500 amu. Comparison between the relative index and mass spectra obtained to that of the available standards in the GCMS library of NIST, Gaithersburg, Maryland, USA, led to identifying compounds in the extract (Leiss et al. 2011).

Nuclear Magnetic Resonance (NMR) spectroscopy

An NMR spectrometer (Bruker advance III 400 MHz) was used to obtain the ^1H NMR spectra of the isolated molecule at the Vellore Institute of Technology, Vellore, India. The solvent used for analysis was DMSO. Chemical shifts were expressed as parts per million (į scale) (Hoeksma et al. 2019).

Bioactive efficacy of the isolated secondary metabolites

Anticancer activity

MTT assay was used to determine anticancer activity as described previously by (Geesala et al. 2016). Anticancer analysis of the fungal extracts and fractions were studied by using different human cancer cell lines such as prostate cancer (*DU-145*), liver cancer (*HepG2*), primary control cell line (*HEK-293*), breast cancer (*MDA-MB-231, MDA-MB-468*, and *MCF-7*), and lung cancer (*A-549*). Cells were briefly trypsinized, and 5×10^3 cells per well were seeded in a 96-well plate. After 24h of incubation, cells were treated with increasing concentrations (0.1, 1, 10, and 100 mg/mL) of all the column fractions, viz. water, chloroform, toluene, ethyl acetate, acetonitrile, and methanol for 48 h followed by fixation of the treated cells along with their respective vehicle controls. The optical density was measured at 510 nm using a multimode reader (Perkin Elmer, Germany), and percent inhibition with IC_{50} was calculated using the Graph pad prism described by Manupati et al. (2019).

DNA fragmentation apoptosis assays

Luminal and Triple Negative Breast Cancer cells, *MCF-7* and *MDA-MB-231*, respectively, were seeded at a density of 0.5×10^6 cells for 24h in complete media to assess the degree of apoptosis induced by the various fractions of *F. oxysporum ABRF1*. Fractions B and C were excluded from further assays as they exhibited cytotoxicity against control *HEK293* cells. The cells were then treated for 24 h with the fractions (50 µg/mL) and positive control, doxorubicin (0.543 µg/mL). After incubation, DNA was extracted from the apoptotic cells using a standard protocol as described previously (Matassov et al. 2004). The concentration of DNA was quantified using a NanoDrop-1000 spectrophotometer (NanoDrop, Wilmington, USA), and 5 µg of DNA was loaded in 1% agarose gel containing ethidium bromide, electrophoresed, and examined under UV radiation to determine DNA fragmentation.

Gene expression analysis

MCF-7 and *MDA-MB-231* were seeded at a density of 0.25×10^6 cells for 24h in a 6-well plate, followed by treatment using the fractions and/or doxorubicin for 24h. Total RNA was extracted using RNA iso plus (Takara Bio, Shiga, Japan), and the mRNA present in the total RNA was used as a template for cDNA synthesis (Puregene, Delhi, India). qRT-PCR analysis of various apoptotic genes was performed using human-specific primers and eukaryotic 18S rRNA as an internal control.

Immunoblot analysis

MDA-MB-231 cells were seeded with 0.5×10^6 cell density and exposed to various fractions and/or doxorubicin for 48h. Total protein was extracted using RIPA lysis buffer supplemented with a protease inhibitor cocktail (Puregene, Delhi, India) and subjected to SDS-PAGE. The protein was then transferred to a PVDF membrane and probed for the presence of apoptotic markers BAX, BCL2, and cleaved Caspase3 (Cell Signaling Technologies, Boston, USA). The β-tubulin expression served as the loading control. Bands were visualized using HRP-based chemiluminescence in a G: Box (Syngene, USA). The density of bands in the obtained images was analyzed using NIH ImageJ software after normalization against β-tubulin.

Molecular docking in silico studies

The interaction of 2-Propenoic acid, pentadecyl ester with anticancer signaling pathways was analyzed by the Molecular Operating Environment (MOE) software compendium (licensed and owned by Chemical Computing Group, Montreal, Canada) (Naik et al. 2011). The targeted protein structures were retrieved from the Research Collaboratory for Structural Bioinformatics (RCSB PDB). Molecular modeling was performed using the docking package *Induced Fit*, a refinement method of MOE (Huo et al. 2020). Protonate 3D application of the software-enabled addition of hydrogen and partial charges to the system

eliminated the bond length and angle biases. A Gaussian surface was generated by Surface and Maps, which was available in the Compute feature, which rendered the binding site and removed the backbone.

MOE/Compute/Simulations/Dock was the location for performing docking. Still, it was based on specific parameters, which were set manually. Hence, the residues close to the ligand atoms defined the docking site, and refinement in the force field minimized the energy in the receptor pocket. The database browser was generated with an S field with the calculated binding free energy identical to the E_refine score. RMSD (root mean square deviation) score was also developed, which quantitatively measured the similarity between two superimposed atomic coordinates. The ligand interaction feature generated the interaction map between the ligand and the receptor's active site, deciphering the participating amino acids and involving chemical bonds.

Focal Adhesion Kinase (RCSB PDB ID: 1MP8), C-Myc promoter (RCSB PDB ID: 6AU4), Vimentin coil 1A/1B (RCSB PDB ID: 3SSU), and TOM1 protein (RCSB PDB ID: 1ELK) were selected as targets for anticancer analysis as these are major components of cellular growth and division and can be modulated by metabolites to regulate their activity.

Statistical analysis

Data were presented as the mean ± standard deviation (SD, n = 3). Statistical difference between various groups was determined by One-Way Analysis of Variance (ANOVA) followed by Duncan multiple range tests. P values ≤ 0.05 were considered statically significant.

RESULTS AND DISCUSSION

Taxonomic, phylogenetic, and biochemical properties of the isolated fungus

Based on morphological and molecular characterization, the fungal isolate ABRF-1 was identified as *F. oxysporum.* The crude extract from the *F. oxysporum* (Figure 2.A) was further analyzed for its chemical compounds using spectroscopic techniques. Biochemical analysis of the crude extract and ethanol acetate, toluene, methanol, chloroform, and acetonitrile fractions was performed. The alkaloid, carbohydrate, cardiac glycosides, coumarins, cyanogenic glycosides, emodins, polyose, polyuronide, and anthraquinones were observed in respective fractions. Chloroform and acetonitrile fractions were rich in biomolecules, as represented in Table 1. One potent compound detected using the standard mass spectrometry databases (Mass Centre and Xcalibur software) (Figure 2.B) was 2-propenoic acid, pentadecyl ester.

Characterization of fungal compounds

Analysis of secondary metabolites using TLC

Fraction on TLC separation has fluorescent spots (spots A and B) with the Rf value of 0.281 (A1) and 0.351 for spot A2. Spots B3-B5 had retention times of 0.233, 0.252, and 0.334. respectively (Figure 2.C).

Identification of fungal secondary metabolites using HPLC

The HPLC analysis of *F. oxysporum* fungus with gradient elution showed nine peaks in spectra of ethanolic extract (Figure 1.A). The peaks with the voltage of 0.5167, 2.5833, 2.8333, 3.55, 3.9, 4.6667, 4.9167, 5, and 9.1333 were observed, and the compound with Rf values of 2.8667 and 3.0833 (Table 2).

GC-MS analysis of the compound isolated from *Fusarium oxysporum ABRF1*

GC-MS analysis of the ethanolic fungal extract and its purified fractions indicated the presence of six major peaks (Figure 1.B). Components and their respective peaks are presented in Table 3. 2-propenoic acid, pentadecyl ester, was the metabolite that was selected to test for its biological activity l. The molecular weight of the compound 2-propenoic acid, pentadecyl ester, was 282 kDa (Figure 1.C).

FTIR analysis of pure compounds

Spectral windows of the aqueous and toluene fractions had chemically significant regions corresponding to C-H (3450- 2850cm-1), amide region dominated by C=O amide I and N-H amide II (Table 4). Furthermore, it also included protein and peptides (1800-1500 cm^{-1}), mixed region (1500-1200 cm^{-1}), polysaccharides region (1200-900 cm^{-1}), and true fingerprint region (900-700 cm^{-1}) (Figure 1.D-E).

Table 1. Secondary metabolites in the fractions of *F.oxysporum* and their respective rich column fraction

Test	Toluene	Chloroform	Ethyl acetate	Methanol	Acetonitrile
Alkaloid Test	+	++++	+	-	++++
Carbohydrate	-	++++	+	-	++++
Cardiac glycosides	-	+++	++	++	++
Coumarins	+	++++	++	+	+++
Cyanogenic glycosides	-	-	-	-	-
Emodins	-	++++	+	+	+++
Polyoses	-	+++	++++	+	+++++
Polyuronoids	+	+++++	++	++	+++++
Anthraquinones	-	-	-	-	-

Note: -: Absent, +: Present, ++: Low concentration, +++: High concentration, ++++: Very high concentration, +++++: Very very high concentration

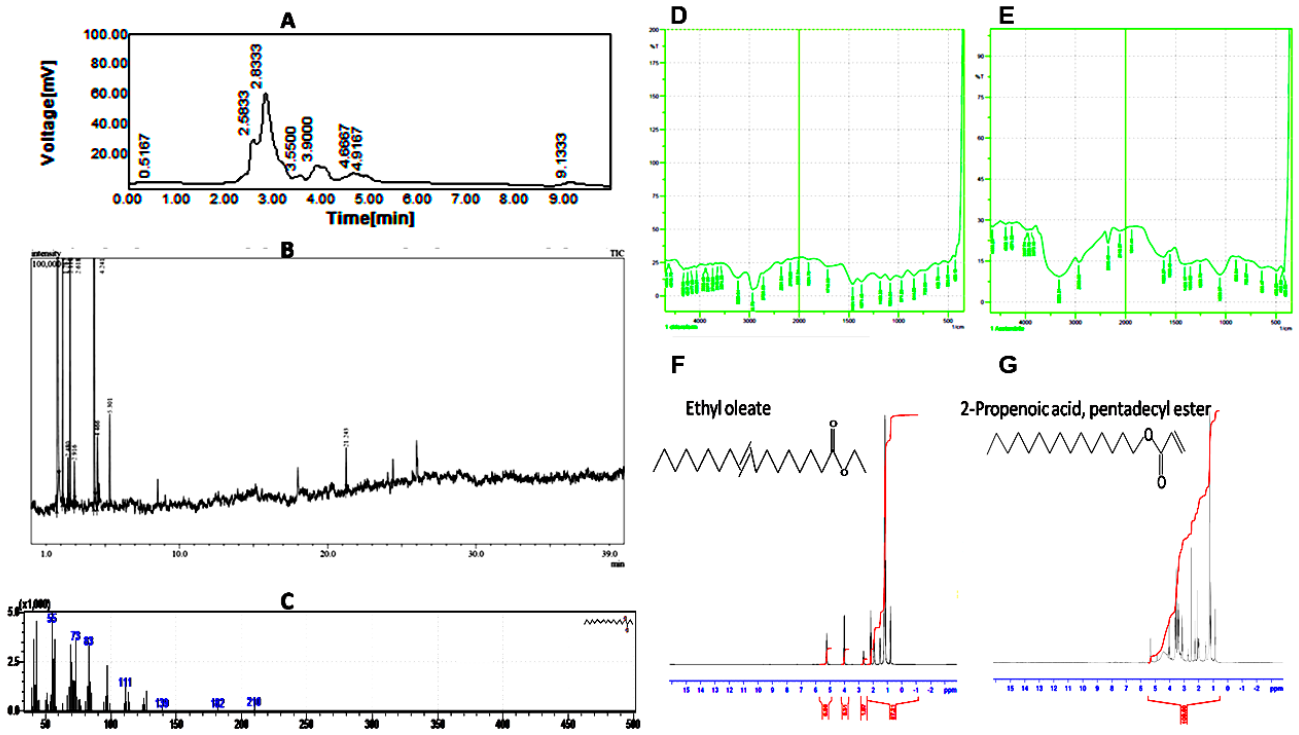

Figure 1. Structure elucidation of 2-propenoic acid, pentadecyl ester with different spectroscopic methods (A) High-Performance Liquid Chromatography (HPLC) chromatogram profile of *Fusarium oxysporum* extract, (B) Chromatogram profile of the *F. oxysporum* extract using GC/MS analysis, (C) Mass spectrum depicting the molecular weight of 2-propenoic acid, pentadecyl ester, (D) FTIR spectrum of chloroform, (E) acetonitrile fractions of column fraction of strain *ABRF1*, and (F) NMR spectrum of the standard ethyl oleate compared with (G) the obtained compound 2-propenoic acid, pentadecyl ester

Table 2. Representing retention time of different secondary metabolites by HPLC analysis

Peak no	RT [min]	Area[mV*sec]	Area%	Height[mV]	Height%
1	0.51	2.90	0.14	0.059	0.05
2	2.58	314.92	14.79	29.40	24.55
3	2.83	1,206.00	56.62	60.34	50.37
4	3.55	68.09	3.20	5.54	4.63
5	3.90	272.76	12.81	11.63	9.71
6	4.66	152.82	7.18	6.21	5.19
7	4.91	50.061	2.35	4.48	3.74
8	9.13	62.36	2.93	2.10	1.76
		2,129.95		119.78	

Table 3. Showing retention time of obtained secondary metabolites and suggesting their possible name by GCMS library of NIST

Peak	R. Time	Area	Height	Name
1	1.78	34,815,263.00	10,119,374.00	Ethanol
2	2.11	114,479.00	90,047.00	Allyl fluoride
3	2.48	25,042.00	17,032.00	Ethyl acetate
4	2.61	248,635.00	171,088.00	1-propanol, 2-methyl
5	2.91	20,774.00	14,772.00	Ethanol, 2-nitro
6	4.24	468,393.00	225,979.00	Ethane, 1, 1-diethoxy
7	4.46	62,871.00	24,547.00	1-butanol, 3-methyl
8	5.30	70,597.00	31,554.00	Toluene
9	21.24	21,897.00	14,406.00	2-propenoic acid, pentadecyl ester
		35,847,951.00	100.00	

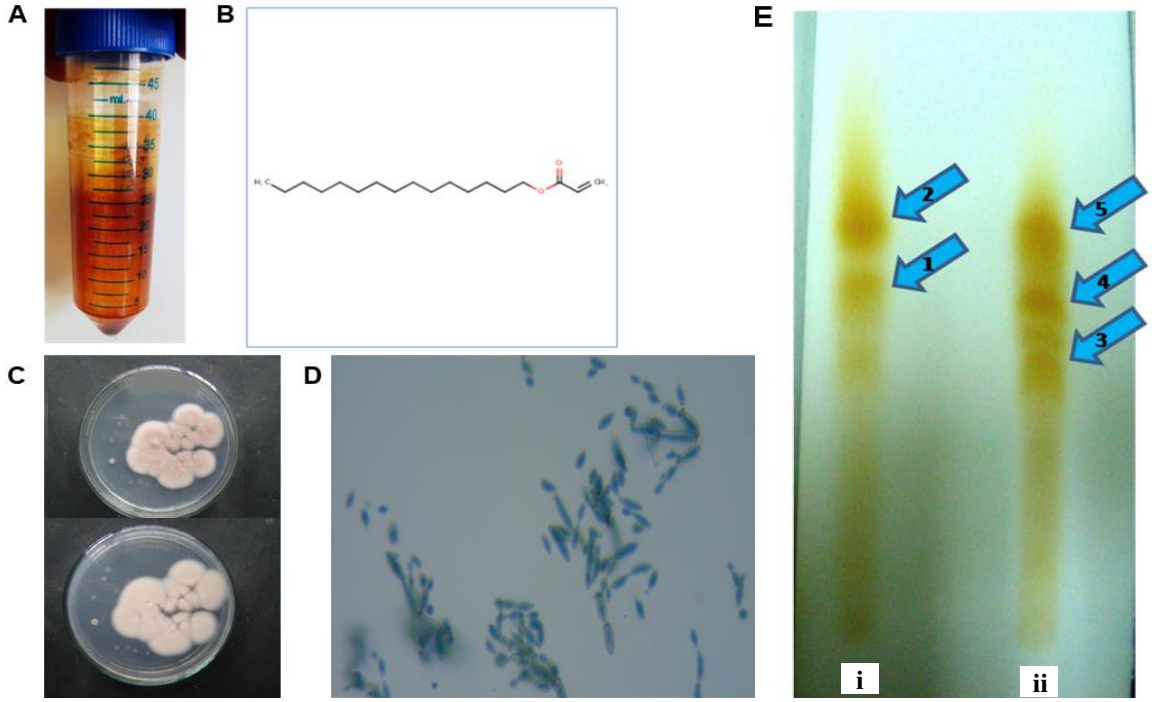

Figure 2. Isolation and Characterization of Secondary Metabolites from *Fusarium oxysporum* (A) Crude extract obtained from the fungus *Fusarium oxysporum* ABRF1 (B) Predicted structure of 2-propenoic acid, pentadecyl ester (C) Colony morphology of the isolated *Fusarium* sp. ABRF1 (both front and back views) (D) Micrograph illustrating the morphological characteristics of *Fusarium* sp. ABRF1 (E) Chromatogram of the (i) chloroform and (ii) acetonitrile soluble fractions obtained from the ethanolic extract of *Fusarium oxysporum*

^{1}H NMR

Column fractions were subjected to structural characterization using the NMR spectrum, and the following peaks were observed at a mixture of į values of proton ^{1}H. The antibacterial activity compound of the secondary metabolite may be due to the presence of methyl, ketone, and hydroxyl functional groups, as predicted from the data. ^{1}H NMR spectrum exhibited the presence of functional groups such as CH2, CH3, OH, and C-H protons. Primary data of the compound of the isolated compound showed the presence of Carbon, Hydrogen, and Hydroxyl groups from the ^{1}H NMR spectrum, which are indicative of ester 2-propenoic acid, pentadecyl ester being (Figure 1.F). This compound also showed the presence of a wide peak at 0.9, 1.3, and 1.5δ, which are primary, secondary, and tertiary aliphatic clusters, respectively. The carbonyl groups at 2.2δ and one of the hydroxyl groups were intact at 3.5, and a few other chemical shifts were also observed. The esters group at 4.1δ confirmed the presence of 2-propenoic acid, pentadecyl ester (Figure 1.G).

Anticancer activity

The intracellular and extracellular secondary metabolites of *ABRF1* and the ethanolic fraction were screened for cytotoxicity against *MCF-7*, *MDA-MB-231*, *DU-145*, *HepG2*, and *A549* cell lines. The extracellular fraction was more potent than the intracellular fraction in inhibiting all cell lines except HepG2 (Table 5). This finding corroborates that most microbes use their extracellular metabolites to communicate with their environment and release these metabolites in response to stress. The ethanolic fraction was highly effective in controlling the proliferation of *DU-145* but did not against *MCF-7*, *MDA-MB-231*, *HepG2*, and *A549* cells (Table 5).

Fraction A (aqueous fraction) had moderate anticancer potential against the *DU-145* prostate cancer and HepG2 liver cancer cell lines with IC_{50} values of 26.2 and 38.8 µg/mL, respectively. However, fraction B (methanol fraction) was moderately potent against the *MCF-7* breast cancer cell line with an IC_{50} value of 24.2 µg/mL. Fraction C (chloroform fraction) had an IC_{50} of 9.4 µg/mL against MDA-*MB-468.* Fraction D (toluene fraction) was moderately active against *MCF-7* with an IC_{50} value of 33.4 µg/mL). The results showed the presence of anticancer components in the fraction of *F. oxysporum ABRF1* with low toxicity against *HEK-293* normal primary cells, except fractions B and C (Table 6).

Apoptosis assays

DNA fragmentation analysis

DNA fragmentation indicates early apoptosis in which cellular endonucleases cleave genomic DNA into fragments between the nucleosomes. After treatment with various fractions, the DNA integrity was obtained in MCF-7 and MDA-MB-231 cells. Fractions D and E caused DNA damage in *MCF-7* cells, while fractions A, D, and E caused DNA cleavage in *MDA-MB-231* cells (Figure 3).

Gene expression analysis

TP53 expression was significantly upregulated by fraction A in *MCF-7* and fractions A and E in *MDA-MB-231* cells (Figure 4.A). Fractions A, D, and F significantly downregulated the expression of a *BCL2* anti-apoptotic gene (Figure 4.B) in *MDA-MB-231* cells. In the *MCF-7* cells, fractions A and D treatment resulted in significant upregulation of both *BID* (Figure 4.C), *BAD* (Figure 4.D), and *BAX* (Figure 4.E). Fractions A and D stimulated the expression of *CASP9* in both *MCF-7* and *MDA-MB-231* (Figure 4.F). Interestingly, significant upregulation of the expression of pro-apoptotic genes was observed in the *MDA-MB-231* after treatment of positive control, doxorubicin.

Protein markers

The gene expression results were further corroborated using immunoblot analysis (Figure 5.A). The anti-apoptotic marker, BCL2 (Figure 5.B), was downregulated in all fractions. In contrast, the pro-apoptotic marker, BAX (Figure 5.C), was significantly upregulated in *MDA-MB-231* cells treated with fraction D. Fraction D also exhibited upregulation of cleaved Caspase3 compared to untreated cells normalized against control β-tubulin (Figure 5.D).

In silico anticancer analysis by Molecular Docking

The binding energy score mimics the potential energy change when the protein and ligand come together. This means that a very negative score corresponds to a strong binding, and a less negative or even positive score corresponds to a weak or non-existing binding. The binding energy or ΔG_{bind} value for target 1MP8 (specific for *MCF-7*) was classified as transferase, i.e., a protein kinase was found to be -10.2313 KCal/mol with 2-propenoic acid, pentadecyl ester specifically at Site 2, and with doxorubicin, it showed the best ΔG_{bind} i.e., -26.9348 kCal/mol (Fig. 4A). The direct bond-forming residues on the active site were Ala 549, Leu 507, Lys 561, Val 554, Gly 563, Asp 546 Trp 588, Glu 614, and Ala 548.

The binding energy for target 1ELK was observed to be -11.3677 KCal/mol with 2-propenoic acid, pentadecyl ester specifically for Site 1, and that of doxorubicin (maximum affinity) and noscapine had lower binding energy scores of -26.9388 KCal/mol and -19.5897 KCal/mol, respectively. Hydrogen bond formation involved direct interaction with Thr A102, Ile A103, Asn A108, and Lys A62. However, Glu B44, Arg B94, and Asn B91 interacted with molecules via water hydration (Fig. 4B).

The binding energy or ΔG_{bind} value for target 6AU4 (specific against cell line *DU-145*) which forms DNA quadruplex in c-Myc promoter's NHE III1 region was -10.7394 KCal/mol with 2-propenoic acid, pentadecyl ester specifically at Site 2 (Tables 7, 8, and Figure 5.C) as compared with Doxorubicin (-15.8666 Kcal/mol) and Noscapine (-10.9021 KCal/mol). The amino acids located at the active site of the receptor-ligand interaction were DG B2, DG B11, DG B13, DG B14, DG B15, DG B17, DG B18, DG B19, and DA A22 (Figure 6.C).

The binding energy or ΔG_{bind} value for target 3SSU was observed to be -7.9592 KCal/mol with 2-propenoic acid, pentadecyl ester specifically for Site 1. In comparison, Doxorubicin and Noscapine showed the lowest binding energy score of -10.5860 KCal/mol and -8.6372 KCal/mol, respectively, and maximum affinity with Site 1 (Figure 6.D). Hydrogen bond formation involved direct interaction with residues Leu A164, Asp A167, Asp A162, and Arg A159 (Figure 6.A).

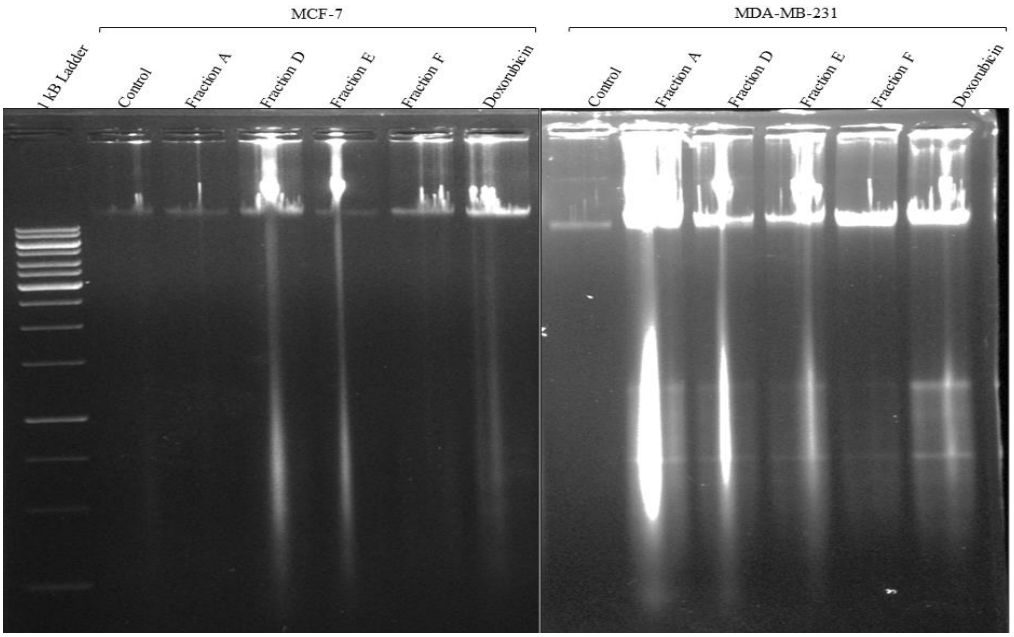

Figure 3. Differential apoptosis of breast cancer cells using DNA fragmentation analysis. Representative photomicrographs depicting DNA fragmentation of MCF-7 (left panel) and MDA-MB-231 (right panel) in presence of various solvent fractions of the isolate, ABRF1. Fraction D and E caused DNA fragmentation in both the types of breast cancer cells. Additionally, fraction A showed marked increase in DNA fragmentation in the MDA-MB-231 cells. Data represented are results of three independent experiments

Table 4. The wavenumber ranges for common functional groups

S. No.	Column Fraction	Wavenumber (cm^{-1})	The Functional Group Identified/Peak Description
1	Obtained peak from acetonitrile fraction of isolate ABRF1	1058.97	CH_2 rocking
2		1058.97	C-O stretching
3		1253.78	C-Oh rocking C-C stretching due to carboxylic acid, ether alcohol, and esters
4		1356.02	C-H scissoring and bending vibrations
5		1406.17	COO- symmetric stretching
6		1620.27	NH_3^+ asymmetric deformation
7		1941.44	NH_3^+ asymmetric deformation
8		2349.4	C-O bond
9		2933.85	CH_2 Asymmetric stretching
10		3328.31	O-H stretching vibration of hydroxyl groups
11		3875.16	O-H stretching-free hydroxyl
12		3939.78	O-H stretching-free hydroxyl
13		3967.74	O-H stretching-free hydroxyl
1	Obtained peak from chloroform fraction of isolate ABRF1	1084.04	C-N symmetric stretching
2		1183.38	C-O bond
3		1371.45	O-H bending polysaccharide
4		1461.14	COO- symmetric stretching
5		1710.93	C=O carbonyl stretching of esters
6		1904.79	NH_3^+ asymmetric deformation
7		2025.34	C≡C alkyne stretching
8		2179.66	C≡C stretch due to alkyne
9		2349.4 2361.94	C-O bond
10		2725.53	Not useful
11		2936.75	OH stretch due to carboxylic acid
12		3229.94	OH stretch due to carboxylic acid
13		3574.25	O-H stretching-free hydroxyl
14		3640.8	O-H stretching-free hydroxyl
15		3742.06	O-H stretching-free hydroxyl
16		3877.09	O-H stretching-free hydroxyl
17		3893.48	O-H stretching-free hydroxyl

Table 5. IC_{50} value of intracellular, extracellular metabolites and ethanolic extract of isolate *Fusarium oxysporum ABRF1* against several cancer cell lines

Fungal Extract	IC_{50} (µg/mL)				
	MCF-7	MDA-MB-231	DU-145	HEPG2	A549
Extracellular secondary metabolites	26.09 ± 1.3	23.22 ± 1.15	15.66 ± 0.78	1807.5 ± 375.57	31.75 ± 1.5
Intracellular secondary metabolites	≥1000	101 ± 5	≥1000	830.45 ± 1.13	≥1000
Ethanolic extract	NI	NI	2.3695±0.156	NI	NI

Table 6. IC_{50} value of *F. oxysporum ABRF1* fractions against various cancer cell lines

Fungal Fraction	IC50[a] (µg/mL)						
	MCF-7[b]	MDA-MB-468[c]	MDA-MB-231[d]	DU-145[e]	HepG-2[f]	A-549[g]	HEK-293[h]
Fraction A	150.23±7.25	136.5± 6.86	106.41±14.61	26.21±4.29	38.8±5.43	89.13±3.16	NI
Fraction B	24.17±6.94	107.03±7.79	82.68±19.24	60.98±11.18	103.86±9.61	58.92±19.81	135.4±9.636
Fraction C	176.16±23.9	9.37±3.66	NI	192.46±17.02	441.56±72.6	149.79± 35.20	173.16±14.67
Fraction D	33.43±6.55	163.45±5.99	67.45±17.90	67.45±17.90	130.13±8.62	47.96±4.19	NI
Fraction E	54.04±8.02	66.81±5.32	61.19±10.92	987.33±104.14	334.56±144.76	56.64± 13.49	NI
Fraction F	110.34±12.8	75.53±4.53	59.95±9.61	85.63±22.94	252.63± 48.97	51.80±11.49	NI

Note: NI: No inhibition; Fractions A: Water; B: Methanol; C: Chloroform; D: Toluene, E: Ethyl acetate, F: Acetonitrile. Note: [a]50% inhibitory concentrations and mean ± SEM of IC50 (µg/mL) values of different fractions represent the mean of three individual experiments: [b]Luminal-A (ER+/PR+/Her2−) breast cancer; [c]Basal (low claudin) triple-negative (ER−/PR−/Her2−) breast cancer; [d]Basal triple-negative (ER−/PR−/Her2−) breast cancer; [e]Moderate metastatic potential (PSA+) androgen-independent prostate cancer; [f]Liver hepatocellular carcinoma; [g]Adenocarcinoma human alveolar basal epithelial cells lung cancer; [h]Non-cancerous primary human embryonic kidney cells

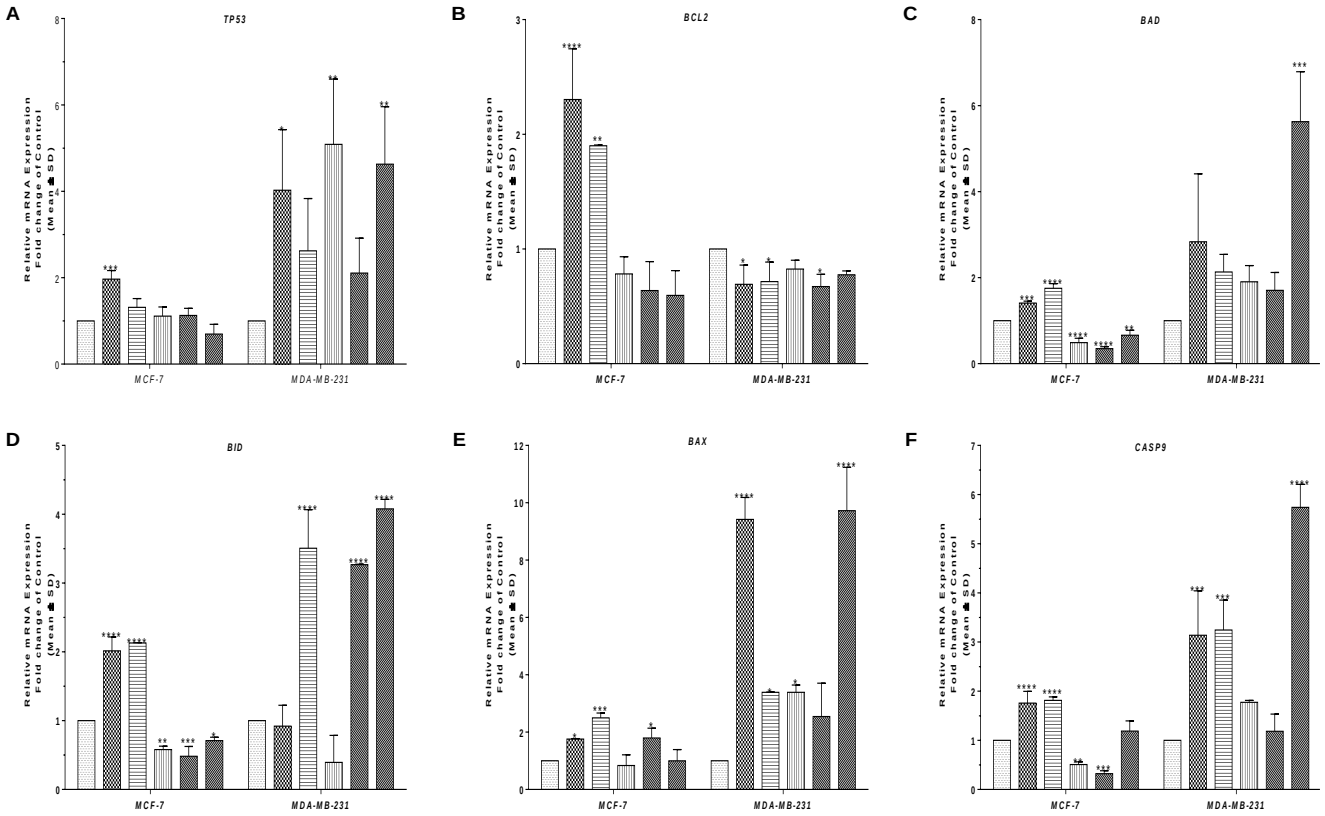

Figure 4. Differential apoptotic marker expression profile. Graphs show the gene expression profile of (A) TP53, (B) BCL2, (C) BAD, (D) BID, (E) BAX, and (F) CASP9 in luminal MCF-7 and TNBC MDA-MB-231 breast cancer cell lines upon treatment with various fractions of ABRF1. Data represented are results of experiments repeated thrice (*p ≤ 0.05, **p ≤ 0.01 ***p ≤ 0.001 and ****p ≤ 0.0001 as compared with their respective control)

Table 7. *In silico* anticancer studies of the compound with different targets in respect of binding energy and number of direct contacts (all polar, non-polar interactions)

Compound Name	Therapeutic Studies	Max Affinity with Site	Binding Energy (kCal/mol)	No. of Direct Contacts (All Polar, Non-Polar Interactions)
2-propenoic acid, pentadecyl ester with 6AU4: DNA	Anticancer study	Site-2	-10.7394	DG B2, DG B11, DG B13, DG B14, DG B15 DG B17, DG B18, DG B19, DA A22 (direct contacts).
2-propenoic acid, pentadecyl ester with 1MP8: Transferase		Site-2	-10.2313	Ala 549, Leu 507, Lys 561, Val 554, Gly 563, Asp 546 Trp 588, Glu 614, Ala 548 (direct contact).
2-propenoic acid, pentadecyl ester with 3SSU		Site-1	-7.9592	Leu A164, Asp A167, Asp A162, Arg A159 (direct contact).
2-propenoic acid, pentadecyl ester with 1ELK		Site-1	-11.3677	Glu B44, Arg B94, Asn B91 (water hydration). Thr A102, Ile A103, Asn A108, Lys A62 (direct contact).

Table 8. A comparison between binding energy score in kCal/mol for the compound 2-propenoic acid, pentadecyl ester in anticancer targets active site and to identify the probable mechanism of action

Molecule	Binding Energy (kCal/mol) of Different Targets for Anticancer Molecular Docking			
	6AU4 (SITE 2)	1MP8 (SITE 2)	3SSU (SITE 1)	1ELK (SITE 7)
Doxorubicin	-15.8666	-26.9348	-10.5860	-26.9388
Noscapine	-10.9021	-18.8507	-8.6372	-19.5897
Pentadecyl acrylate	-10.7394	-10.2313	-7.9592	-11.3677

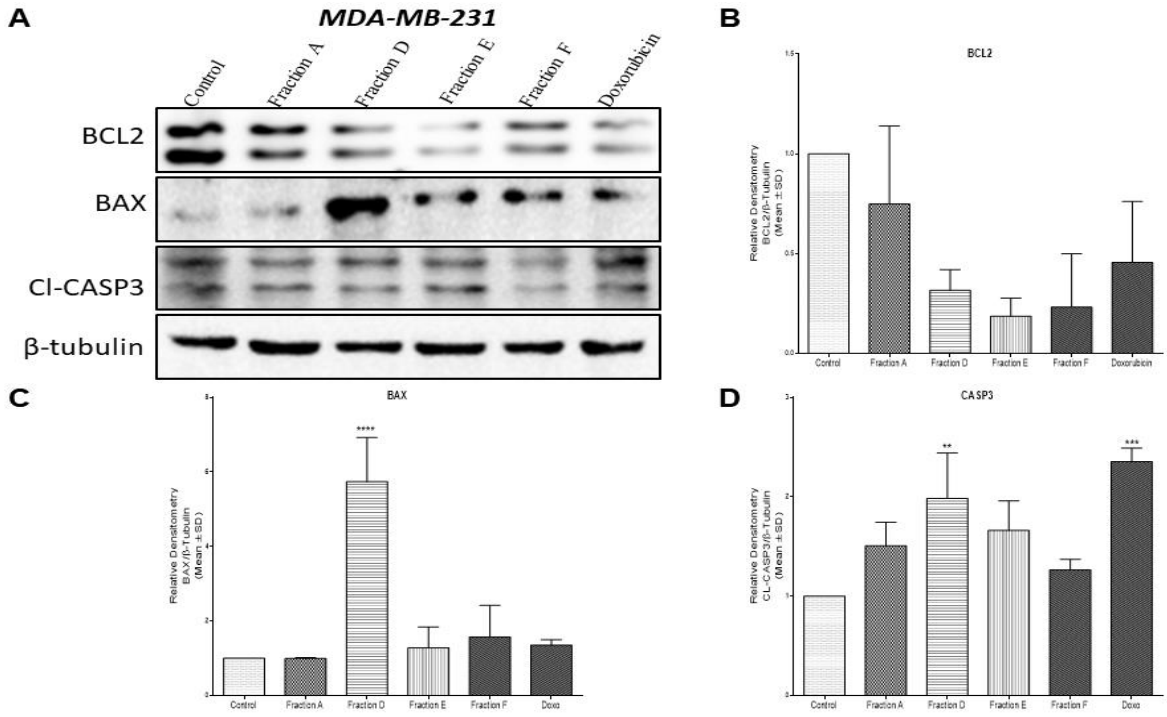

Figure 5. Apoptotic protein expression analysis. (A) Representative image of immunoblot analysis of MDA-MB-231 cells treated with various fractions of ABRF1 and positive control doxorubicin. Quantification of protein bands (B) BCL2, (C) BAX, and (D) Cl-CASP3 using NIH ImageJ software normalized against internal loading control β-tubulin. Data are represented as mean ± SD from three replicates, $^{**}p \leq 0.01$ $^{***}p \leq 0.001$ and $^{****}p \leq 0.0001$ compared to control

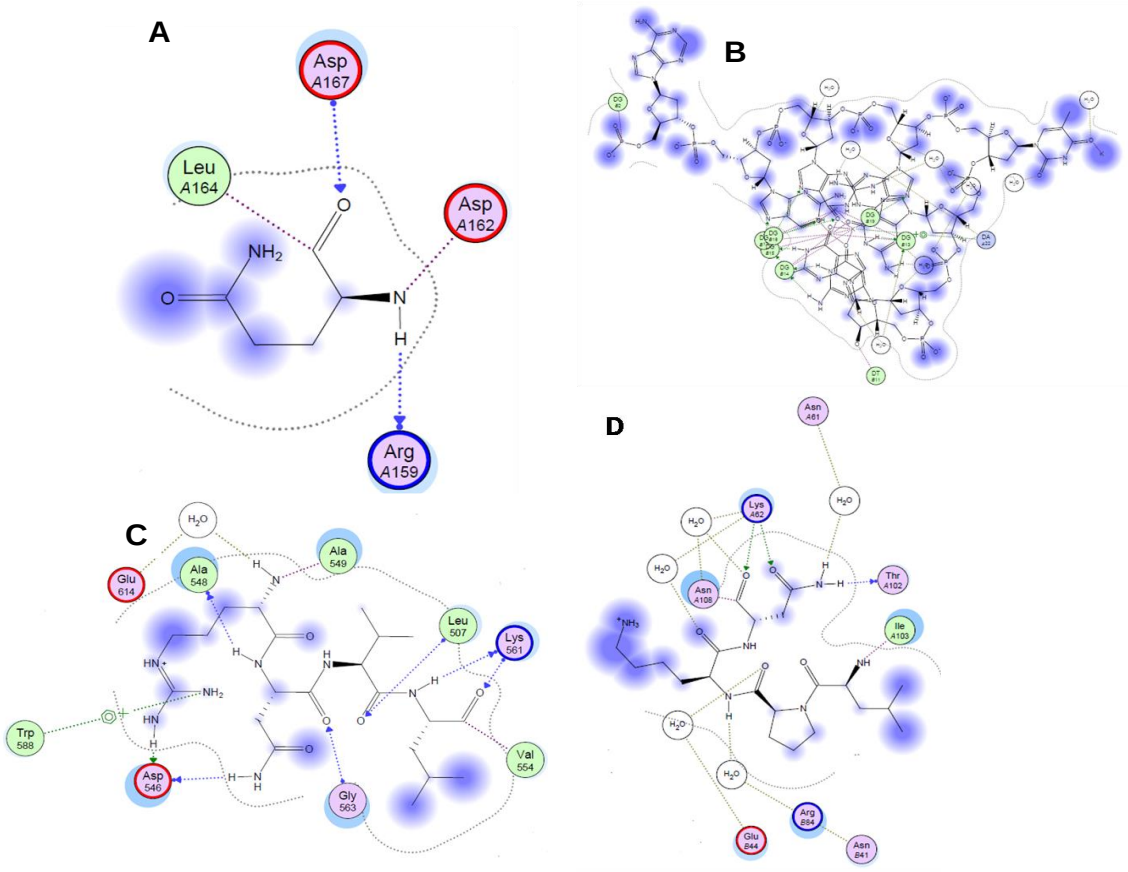

Figure 6. Molecular docking and 2D interaction diagram of 2-propenoic acid, pentadecyl ester.Interactions of 2-propenoic acid, pentadecyl ester with (A) major quadruplex formed in the human c-MYC promoter (RCSB ID:6AU4), (B) Focal Adhesion Kinase (FAK) (RCSB ID:1MP8), (C) central helical domain of vimentin (RCSB ID:3SSU), and (D) VSH domain of TOM1 (RCSB ID:1ELK).

Discussion

The present study isolated and characterized bioactive secondary metabolites from *F. oxysporum ABRF1)* (Wyatt et al. 2013; Gautier et al. 2016). The bioactive metabolites of the crude extract from the *F. oxysporum* were identified using TLC, HPLC, and FTIR. The structure of the bioactive molecule was identified as 2-propenoic acid, pentadecyl ester, using the standard mass spectrometry databases viz. GC-MS and NMR. The secondary metabolite was hypothesized to have drug-likeliness based on SWISS ADME and moderate solubility in water. Based on the BOILED-Egg model, the 2-propenoic acid pentadecyl ester was predicted to be actively absorbed through the gastrointestinal tract and penetrate the blood-brain barrier. The molecule is a lead candidate with a carrier required for drug targeting.

The isolated bioactive metabolite was evaluated for anticancer properties mainly focused on DNA fragmentation apoptosis assay, gene and protein expression analysis, and *in silico* validation with molecular docking studies. The secondary metabolite from *F. oxysporum ABRF1)* led to DNA fragmentation that was observed as a smear and not in the distinctive ladder pattern of 180-200 bp fragments as the cells underwent apoptosis asynchronously (Matalová and Španová 2002). Fragmentation of nuclear DNA triggers the intrinsic apoptotic pathway in the cell. The interactions between various members of BCL2, anti-apoptotic - BCL2, and pro-apoptotic markers – p53 that initiate oligomerization sensitizer – BAD, activator - BID, and pore-former – BAX cause increased mitochondrial outer membrane permeability and release of cytochrome-c into the cytosol. Cytochrome C initiates the caspase cascade that digests proteins needed for cellular functioning and triggers apoptosis (Kale et al. 2018). Cyt C oligomerizes with APAF1 in the cytoplasm to form the apoptosome that activates Caspase9, activating the executioner Caspase3 and triggering cell death (Ledgerwood and Morison 2009).

Several diseases, such as inflammation, carcinomas, and metabolic pathways, have been targeted using inhibitors of protein kinases (Bhullar et al. 2018). EphA2 (Ephrin receptor A2), Aurora-A, and FAK (focal adhesion kinase) are protein kinases reported to be involved in cancer. High expression profiles of these protein kinases in human tumors suggest that their inhibitors may be a potent candidate for cancer treatment (Gross et al. 2015). TOM1 protein or Target of Myb protein 1 is reported to play a vital role in processes such as intracellular trafficking, the dilapidation of GFR (growth factor receptor) complexes through translocation into the lysosome, endocytosis, neutrophil degranulation, and endosomal & protein transport (Keskitalo et al. 2019). TOM1 is a potential target against the *MCF-7* breast cancer cell line (Chevalier et al. 2016).

Fusarium species are a significant source of cytotoxic metabolites, e.g., camptothecin, taxol, baccatin III, phelligridin B, and metacytofilin (Noman et al. 2021; Tapfuma et al. 2019). The initial screening of the fractions of *F. oxysporum* isolate-*ABRF1* showed anticancer potential. Subsequently, a differential cytotoxic profile of the various fractions was observed against several cancer cell lines. The suspected mechanism of cytotoxic activity of these fractions was assessed by analyzing their impact on DNA fragmentation, apoptosis-related genes, and protein expression. DNA fragmentation indicates early apoptosis, wherein endonucleases break down genomic DNA into fragments between the nucleosomes. Fragmentation of nuclear DNA triggers the intrinsic apoptotic in the cell. One of the common therapeutic fungi, the *Ganoder macurtisii strain* (GH-16-015), showed anticancer activity against a wide range of cancer cell lines - *A549*, *HBL-100*, *HeLa*, and *T-47D* (Serrano-Márquez et al. 2021). Altersolanol B from *Stemphylium solani* induced intrinsic apoptosis in *MCF-7* cells through downregulation of anti-apoptotic BCl-2 and upregulation and activation of caspase 9, poly (ADP-ribose) polymerase (PARP) and pro-apoptotic Bax (Siraj et al. 2022). The results of this study showed that the identified secondary metabolite, 2-propenoic acid, pentadecyl ester downregulated the expression of an anti-apoptotic marker, BCL2, and upregulated the pro-apoptotic markers - *BID*, *BAD*, *BAX*, and *Caspase9*. The anticancer properties of the metabolites may be attributed to the binding of these molecules with specific targets and their consequent modulation to regulate metabolic and molecular processes.

The present study further validated the proposed mechanism by protein marker assay and molecular docking analysis. The protein markers corroborated the gene expression results, showing the downregulated BCL2 and significantly upregulated BAX and activation by cleavage of Caspase 3 in *MDA-MB-231* cells. The identified secondary metabolite, 2-propenoic acid, pentadecyl ester, was subjected to molecular docking on selected targets and compared to standard drugs, Doxorubicin and Noscapine. An effective interaction between the secondary metabolite and these cancer-related molecular targets exists. We hypothesize that 2-propenoic acid, pentadecyl ester, interacts with c-myc and other cell cycle regulatory targets and controls DNA double-strand break repair gene expression (Chen et al. 2018). It renders cancer cells prone to DNA damage, consequently inducing apoptosis. The active metabolite 2-propenoic acid, pentadecyl ester, suppresses anti-apoptotic genes and activates pro-apoptotic genes, leading to cytotoxic activity. The molecule may act by a multipronged mechanism on multiple targets. This secondary metabolite is an effective anticancer agent with minimal adverse effects; therefore, it needs further study.

In conclusion, a fungal species isolated from the Achanakmar forest reserve, *F. oxysporum ABRF*1, had high cytotoxicity. We identified a novel secondary metabolite, 2-propenoic acid, pentadecyl ester, with therapeutic potential as an anticancer agent. Further studies are required to evaluate this secondary metabolite's molecular mechanism of action.

ACKNOWLEDGMENTS

An institutional grant supported this work, and the authors are thankful to the Department of Biotechnology,

Guru Ghasidas Vishwavidyalaya, India, for providing the facilities to carry out the research. The work is also supported by UGC SAP project no. F.3-14/2016/DRS-I(SAP-II) and DBT BUILDER (BT/PR 7020/INF/22/172/2012). AD acknowledges the funding provided by DBT, the Government of India, the Cancer Pilot Project, and Sanction No. 6242-P65/RGCB/PMD/DBT/AMTD/2015. Funding provided by CSIR JRF/SRF to SS and DS is acknowledged gratefully. (Manuscript Communication no. IICT/Pubs./2021/217).

REFERENCES

Alkhulaifi MM, Awaad AS, Al-Mudhayyif HA, Alothman MR, Alqasoumi SI, Zain SM. 2019. Evaluation of the antimicrobial activity of secondary metabolites of fungi isolated from Sultanate Oman soil. Saudi Pharm J 27 (3): 401-405. DOI: 10.1016/j.jsps.2018.12.009.

Arnott JA, Planey SL. 2012. The influence of lipophilicity in drug discovery and design. Expert Opin. Drug Discov 7: 863-875. DOI: 10.1517/17460441.2012.714363.

Azerang P, Khalaj V, Kobarfard F, Owlia P, Sardari S, Shahidi S. 2019. Molecular characterization of a fungus producing membrane-active metabolite and analysis of the produced secondary metabolite. Iranian Biomed J 23 (2): 121. DOI: 10.29252/.23.2.121.

Bakker PA, Pieterse CM, de Jonge R, Berendsen RL. 2018. The soil-borne legacy. Cell 172 (6): 1178-1180. DOI: 10.1016/j.cell.2018.02.024.

Berg M, Koskella B. 2018. Nutrient- and dose-dependent microbiome-mediated protection against a plant pathogen. Curr Biol 28 (15): 2487-2492. DOI: 10.1016/j.cub.2018.05.085.

Bhat R. 2013. Potential use of Fourier transform infrared spectroscopy for identification of molds capable of producing mycotoxins. Intl J Food Prop 16 (8): 1819-1829. DOI: 10.1080/10942912.2011.609629.

Bhullar KS, Lagarón NO, McGowan EM, Parmar I, Jha A, Hubbard BP, Rupasinghe HP. 2018. Kinase-targeted cancer therapies: Progress, challenges, and future directions. Mol Cancer 17 (1): 1-20. 10.1186/s12943-018-0804-2.

Braga RM, Dourado MN, Araújo WL. 2016. Microbial interactions: ecology in a molecular perspective. Braz J Microbiol 47: 86-98. DOI: 10.1016/j.bjm.2016.10.005.

Castillo-González C, Zhang X. 2018. The Trojan horse of the plant kingdom. Cell Host Microbe 24 (1): 1-3. DOI: 10.1016/j.chom.2018.06.015.

Chen H, Liu H, Qing G. 2018. Targeting oncogenic Myc as a strategy for cancer treatment. Signal Transduc Target Ther 3 (1): 1-7. DOI: 10.1038/s41392-018-0008-7.

Chevalier C, Collin G, Descamps S, Touaitahuata H, Simon V, Reymond N, Benistant C. 2016. TOM1L1 drives membrane delivery of MT1-MMP to promote ERBB2-induced breast cancer cell invasion. Nat Commun 7(1): 1-16. DOI: 10.1038/ncomms10765.

Compant S, Samad A, Faist H, Sessitsch A. 2019. A review on the plant microbiome: Ecology, functions, and emerging trends in microbial application. J Adv Res 19: 29-37. DOI: 10.1016/j.jare.2019.03.004.

Demain AL, Fang A. 2000. The natural functions of secondary metabolites. In: Fiechter A (eds). History of Modern Biotechnology I. Advances in Biochemical Engineering/Biotechnology, vol 69. Springer, Berlin, Heidelberg. DOI: 10.1007/3-540-44964-7_1.

Dreher D, Baldermann S, Schreiner M, Hause B. 2019. An arbuscular mycorrhizal fungus and a root pathogen induce different volatiles emitted by *Medicago truncatula* roots. J Adv Res 19: 85-90. DOI: 10.1016/j.jare.2019.03.002

D'Souza RA, Kamat NM. 2017. Potential of FTIR spectroscopy in chemical characterization of *Termitomyces* pellets. J Appl Biol Biotechnol 5 (4): 080-084. DOI: 10.7324/JABB.2017.50412.

Gautier M, Normand AC, Ranque S. 2016. Previously unknown species of Aspergillus. Clin Microbiol Infect 22 (8): 662-669. DOI: 10.1016/j.cmi.2016.05.013.

Geesala R, Gangasani JK, Budde M, Balasubramanian S, Vaidya JR, Das A. 2016. 2-Azetidinones: Synthesis and biological evaluation as potential anti-breast cancer agents. Eur J Med Chem 124: 544-558. DOI: 10.1016/j.ejmech.2016.08.041.

Gkarmiri K, Mahmood S, Ekblad A, Alstrom S, Hogberg N, Finlay R. 2017. Identifying the active microbiome associated with roots and rhizosphere soil of rapeseed oil. Appl Environ Microbiol 83 (22): 1-14. DOI: 10.1128/AEM.01938-17.

Gross S, Rahal R, Stransky N, Lengauer C, Hoeflich KP. 2015. Targeting cancer with kinase inhibitors. J Clin Invest 125 (5): 1780-1789. DOI: 10.1172/JCI76094.

Hibbing ME, Fuqua C, Parsek MR, Peterson SB. 2010. Bacterial competition: Surviving and thriving in the microbial jungle. Nat Rev Microbiol 8 (1): 15-25. DOI: 10.1038/nrmicro2259.

Hoeksma J, Misset T, Wever C, Kemmink J, Kruijtzer J, Versluis K, den Hertog J. 2019. A new perspective on fungal metabolites: Identification of bioactive compounds from fungi using zebrafish embryogenesis as a read-out. Sci Rep 9 (1): 1-16. DOI: 10.1038/s41598-019-54127-9.

Huo J, Zhong S, Du X, Cao Y, Wang W, Sun Y, Li Y. 2020. Whole-genome sequence of *Phellinus gilvus* (mulberry Sanghuang) reveals its unique medicinal values. J Adv Res 24: 325-335. DOI: 10.1016/j.jare.2020.04.011.

Kaiser R. 2006. Flowers and fungi use scents to mimic each other. Science 311 (5762): 806-807. DOI: 10.1126/science.1119499.

Kale J, Osterlund EJ, Andrews DW. 2018. BCL-2 family proteins: Changing partners in the dance towards death. Cell Death Different 25 (1): 65-80. DOI: 10.1038/cdd.2017.186.

Keskitalo S, Haapaniemi EM, Glumoff V, Liu X, Lehtinen V, Fogarty C, Varjosalo M. 2019. Dominant TOM1 mutation associated with combined immunodeficiency and autoimmune disease. NPJ Genom Med 4 (1): 1-7. DOI: 10.1038/s41525-019-0088-5.

Leach JE, Triplett LR, Argueso CT, Trivedi P. 2017. Communication in the phytobiome. Cell 169 (4): 587-596. DOI: 10.1016/j.cell.2017.04.025.

Ledgerwood EC, Morison IM. 2009. Targeting the apoptosome for cancer therapy. Clin Cancer Res 15 (2): 420-424. DOI: 10.1158/1078-0432.CCR-08-1172.

Leiss KA, Choi YH, Verpoorte R, Klinkhamer PG. 2011. An overview of NMR-based metabolomics to identify secondary plant compounds involved in host plant resistance. Phytochem Rev 10 (2): 205-216. DOI: 10.1007/s11101-010-9175-z.

Lin MT, Mahajan JR, Dianese JC, Takatsu A. 1976. High production of kojic acid crystals by *Aspergillus parasiticus* UNBF A12 in liquid medium. Appl Environ Microbiol 32 (2): 298-299. DOI: 10.1128/aem.32.2.298-299.1976.

Manupati K, Debnath S, Goswami K, Bhoj PS, Chandak HS, Bahekar SP, Das A. 2019. Glutathione S-transferase omega 1 inhibition activates JNK-mediated apoptotic response in breast cancer stem cells. FEBS J 286 (11): 2167-2192. DOI: 10.1111/febs.14813.

Matalová E, Španová A. 2002. Detection of an apoptotic DNA ladder in pig leukocytes and its precision using LM-PCR (ligation-mediated polymerase chain reaction). Acta Veterinaria Brno 71 (2): 163-168. DOI: 10.2754/avb200271020163.

Matassov D, Kagan T, Leblanc J, Sikorska M, Zakeri Z. 2004. Measurement of apoptosis by DNA fragmentation. Methods Mol Biol 282: 1-17. DOI: 10.1385/1-59259-812-9:001.

McGHEE JE, St Julian G, Detroy RW. 1982. Continuous and static fermentation of glucose to ethanol by immobilized *Saccharomyces cerevisiae* cells of different ages. Appl Environ Microbiol 44 (1): 19-22. DOI: 10.1128/aem.44.1.19-22.1982.

Meligy ME, Zain ME, Awaad AS, Othman MR, Alafeefy AM. 2014. Biological activity of fungal secondary metabolites. Intl J Chem Appl Biol Sci 1: 14-22. DOI:10.4103/2348-0734.124359.

Miranda H, Simão R, Santos VP, Salles BF, Pacheco MT, Willardson JM. 2010. Exercise order interacts with rest interval during upper-body resistance exercise. J Strength Cond Res 24: 1573-1577. DOI: 10.1519/JSC.0b013e3181d8ea61.

Naik PK, Chatterji BP, Vangapandu SN, Aneja R, Chandra R, Kanteveri S, Joshi HC. 2011. Rational design, synthesis, and biological evaluations of amino-noscapine: A high-affinity tubulin-binding noscapinoid. J Comput-aided Mol Design 25 (5): 443-454. DOI: 10.1007/s10822-011-9430-4.

Noman E, Al-Shaibani MM, Bakhrebah MA, Almoheer R, Al-Sahari M, Al-Gheethi A, Abdulaal WH. 2021. Potential of anticancer activity of secondary metabolic products from marine fungi. J Fungi 7 (6): 436. DOI: 10.3390/jof7060436.

Pinton A, Varanini Z Nannipieri P. eds. 2010. The Rhizosphere: Biochemistry and Organic Substances at the Soil-Plant Interface. CRC Press, Boca Raton, FL. DOI:10.1007/s10535-009-0039-6.

Radhika KP, Rodrigues BF. 2010. Arbuscular mycorrhizal fungal diversity in some commonly occurring medicinal plants of Western Ghats, Goa region. J For Res 21 (1): 45-52. DOI: 10.1007/s11676-010-0007-1.

Robinson T, Singh D, Nigam P. 2001. Solid-state fermentation: A promising microbial technology for secondary metabolite production. Appl Microbiol Biotechnol 55 (3): 284-289. DOI: 10.1007/s002530000565.

Sahu M, Jha H. 2020a. Study on antioxidant, antidiabetic, and antibacterial activity of rhizospheric fungi from Achanakmar Biosphere Reserve, Bilaspur. Egypt J Microbiol 55 (1): 29-44. DOI: 10.21608/EJM.2020.31025.1160.

Sahu MK Yeeravalli R, Das A, Jha H. 2023a. Secondary metabolites of rhizospheric fungal isolate *Aspergillus carneus* ABRF4 regulate the antibacterial and anti-proliferative activity against cancer cells. Nusantara Biosci 15: 137-142. DOI: 10.1186/s40643-020-00303-z.

Sahu MK, Jha H. 2020b. Rhizospheric fungi: Diversity and therapeutic potential. In: Chaurasia PK, Bharti SL (eds). Research Advances in the Fungal World. Nova Publisher, New York.

Sahu MK, Kaushik K, Das A, Jha H. 2020. In vitro and in silico antioxidant and anti-proliferative activity of rhizospheric fungus *Talaromyces purpureogenus* isolate-ABRF2. Bioresour Bioprocess 7: 14. DOI: 10.1186/s40643-020-00303-z.

Sahu MK, Yeeravalli R, Das A, Jha H. 2023b. Secondary metabolites of rhizospheric fungal isolate *Aspergillus carneus* ABRF4 regulate the antibacterial and anti-proliferative activity against cancer cells. Nusantara Biosci 15 (2): 137-142. DOI: 10.13057/nusbiosci/n150201.

Sarsaiya S, Shi J, Chen J. 2019. A comprehensive review on fungal endophytes and its dynamics on Orchidaceae plants: Current research, challenges, and future possibilities. Bioengineered 10 (1): 316-334. DOI: 10.1080/21655979.2019.1644854.

Serrano-Márquez L, Trigos Á, Couttolenc A, Padrón JM, Shnyreva AV, Mendoza G. 2021. Antiproliferative and antibacterial activity of extracts of *Ganoderma* strains grown in vitro. Food Sci Biotechnol 30 (5): 711-721. DOI: 10.1007/s10068-021-00903-1.

Sharma D, Pramanik A, Agrawal PK. 2016. Evaluation of bioactive secondary metabolites from endophytic fungus *Pestalotiopsis neglecta* BAB-5510 isolated from leaves of *Cupressus torulosa* D. Don. 3 Biotech 6 (2): 1-14. DOI: 10.1007/s13205-016-0518-3.

Shen HY, Jiang HL, Mao HL, Pan G, Zhou L, Cao YF. 2007. Simultaneous determination of seven phthalates and four parabens in cosmetic products using HPLC-DAD and GC-MS methods. J Separation Sci 30 (1): 48-54. DOI: 10.1002/jssc.200600215.

Siraj MA, Jacobs AT, Tan GT. 2022. Altersolanol B, a fungal tetrahydroanthraquinone, inhibits the proliferation of estrogen receptor-expressing (ER+) human breast adenocarcinoma by modulating PI3K/AKT, p38/ERK MAPK, and associated signaling pathways. Chem-Biol Interact 359: 109916. DOI: 10.1016/j.cbi.2022.109916.

Soccol CR, da Costa ESF, Letti LAJ, Karp SG, Wojciechowski AL, de Souza Vandenberghe LP. 2017. Recent developments and innovations in solid-state fermentation. Biotechnol Res Innov 1 (1): 52-71. DOI: 10.1016/j.biori.2017.01.002.

Tapfuma KI, Uche-Okereafor N, Sebola TE, Hussan R, Mekuto L, Makatini MM, Mavumengwana V. 2019. Cytotoxic activity of crude extracts from Daturastramonium's fungal endophytes against A549 lung carcinoma and UMG87 glioblastoma cell lines and LC-QTOF-MS/MS-based metabolite profiling. BMC Complement Alternat Med 19 (1): 1-12. DOI: 10.1186/s12906-019-2752-9.

Vinale F, Sivasithamparam K, Ghisalberti EL, Ruocco M, Woo S, Lorito M. 2012. *Trichoderma* secondary metabolites that affect plant metabolism. Nat Prod Commun 7 (11): 1545-1550. DOI: 10.1177/1934578X1200701133.

Wyatt TT, Wösten HA, Dijksterhuis J. 2013. Fungal spores for dispersion in space and time. Adv Appl Microbiol 85: 43-91. DOI: 10.1016/B978-0-12-407672-3.00002-2.